euronoise

Numerical analysis of airborne and impact sound insulation between non-contiguous acoustic spaces using the Boundary Element Method

Andreia Pereira, António Tadeu and Paulo Santos

University of Coimbra, Department of Civil Engeneering - Pólo II da Universidade - Rua Luís Reis Santos, 3030-788 Coimbra, Portugal
apereira@dec.uc.pt

In this paper a Boundary Element Method (BEM) is used to predict the acoustic behaviour provided by four two-dimensional acoustic closed spaces separated by slabs and walls, surrounded by an elastic infinite medium. The walls and slabs are modelled as single partitions. The model is excited by cylindrical loads in the form of an airborne sound source placed in the acoustic space or an impact sound source acting on the slab, perpendicular to its surface. The BEM algorithm is formulated in the frequency domain using Green's functions for full fluid and elastic media. The formulation is developed following a direct BEM approach which assumes full coupling between the fluid medium and the elastic medium. The model requires the discretization of all interfaces and allows the analysis in the low and medium frequency range.
A numerical analysis is performed to study airborne and impact sound insulation between acoustic non-contiguous spaces, where the sound pressure level which is established in the receiving room is due to flanking transmission. The influence of the structure's stiffness on the sound insulation is discussed for varying thicknesses of the partitions. The acoustic behaviour of the structure is described by sound insulation curves and average vibration velocity level curves of the walls and slabs and the results are discussed.

1 Introduction

The transmission of airborne sound energy through a single separation element depends on several variables, such as the frequency of sound incident on the element, the physical properties of the panel (mass, internal damping, elasticity modulus, Poisson's ratio), the connections with the surrounding structure and the vibration eigenmodes of the element. The prediction of the physical phenomena regarding wave propagation is quite complex, and this has led to several simplified models such as the theoretical Mass Law, which assumes the element behaves like a group of infinite juxtaposed masses with independent displacement and null damping forces. Sewell [1] and Sharp [2] have proposed other simplified models for the frequencies below, in the vicinity of and above the coincidence effect to predict the airborne sound insulation provided by single panels.

It is also important to predict the impact sound insulation provided by partitions at the design stage. The development of a prediction model has to take the excitation and the sound transmission system into account. Several authors have addressed the problem of the excitation source, where the interaction at the interfaces between the hammer and the floor has to be considered. Cremer [3] has derived an impact source spectrum caused by the tapping machine acting on homogeneous floors of high impedance. He assumes that the impact is perfectly elastic and the results were proved to be satisfactory for several frequencies. Vér [4] derived a complete description of the force spectrum and impact level provided by the tapping machine on hard surfaces.

However, to accurate predict airborne or impact sound insulation between two rooms it may be required to take into account all the transmission paths and not only the transmission though the main element (i.e. direct sound transmission). Note also that when sound transmission between no-adjacent rooms is being studied, the final response is due to flanking transmission.

In this paper a numerical analysis is performed to study airborne and impact sound insulation between acoustic non-contiguous spaces, where the sound pressure level which is established in the receiving space is due to flanking transmission. A Boundary Element Method (BEM) developed by the authors is used to predict the acoustic behaviour provided by four two-dimensional acoustic closed spaces separated by slabs and walls, surrounded by an elastic infinite medium. It is the aim of this work to assess how the present model may be used to predict sound insulation including flanking transmission.

The influence of the structure's stiffness on the sound insulation is discussed for varying thicknesses of the separation elements. The acoustic behaviour of the structure is described by sound insulation curves and average vibration velocity level curves of the walls and slabs and the results are discussed.

The next section describes the problem formulation. Follows the numerical simulations and the discussion of the results.

2 Problem formulation

Consider the geometry displayed in Fig. 1 representing a set of 2D acoustic spaces driven through an elastic medium subject to either a harmonic line airborne sound source or an impact source acting on the slab along the vertical direction. The fluid medium with density ρ_f and Lamé constant λ_f, allows the propagation of pressure waves with velocity α_f. In the elastic medium, assumed to have density ρ and shear modulus μ, propagate compressional waves with velocity α and shear waves with velocity β.

The internal material loss is computed by using a complex shear modulus and complex Lamé's constant. The shear modulus is computed as $\mu = \mu_r(1+\mathrm{i}\eta)$, where μ_r corresponds to the classic modulus and η is the loss factor. The complex Lamé's constants can be written in the same form as the Young's modulus.

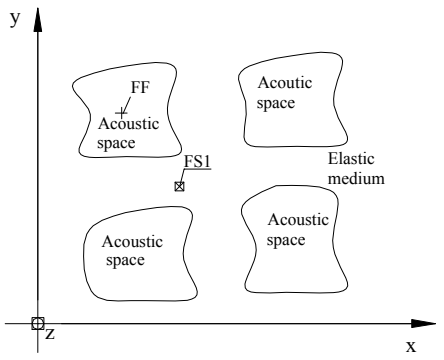

Fig.1 Geometry of the problem.

When the above described system is excited by spatially sinusoidal harmonic line load, acting in the fluid medium (SF) at (x_0, y_0), the incident pressure field at a point (x, y, z) is given in the frequency wave-number domain by:

$$\sigma^{full} = \frac{-\mathrm{i}A}{2}\mathrm{H}_0^{(2)}\left(k_{\alpha_f}\sqrt{(x-x_0)^2+(y-y_0)^2}\right)\mathrm{e}^{-\mathrm{i}k_z z}, \quad (1)$$

in which A is the wave amplitude; ω is the excitation frequency; $\mathrm{i} = \sqrt{-1}$; $k_{\alpha_f} = \sqrt{\omega^2/(\alpha_f)^2 - k_z^2}$ (with $\mathrm{Im}\, k_{\alpha_f} < 0$); k_z is the spatial wavenumber along the z direction ($k_z = \frac{2\pi}{L}m$), and $H_n^{(2)}(...)$ are second Hankel functions of order n.

If a spatially sinusoidal harmonic line load acts at a point (x_s, y_s) of the elastic medium (SS), the resulting incident field can be expressed by the displacements $G_{y,k}^{full}$ (where the index, $k = x, y, z$, indicates the direction of the displacement) at a point (x, y) according to the following expressions [5]:

$$G_{yx}^{full}(\omega, x, y, k_z) = \gamma_x\gamma_y AB_2 \quad (2)$$

$$G_{yy}^{full}(\omega, x, y, k_z) = A\left[\left(\frac{\omega}{\beta}\right)H_{0\beta} - \frac{1}{r}B_1 + \gamma_y^2 B_2\right]$$

$$G_{yz}^{full}(\omega, x, y, k_z) = \mathrm{i}k_z\gamma_y AB_1$$

where $A = \frac{1}{4\mathrm{i}\rho\omega^2}$; $\gamma_i = \frac{\partial r}{\partial x_i} = \frac{x_i}{r}$ and $i = 1, 2$ corresponds to the direction cosines; $B_n = (k_\beta)^n H_{n\beta} - (k_\alpha)^n H_{n\alpha}$; $H_{n\alpha} = \mathrm{H}_n^{(2)}(k_\alpha r)$ and $H_{n\beta} = \mathrm{H}_n^{(2)}(k_\beta r)$; $r = \sqrt{(x-x_s)^2+(y-y_s)^2}$; $k_\alpha = \sqrt{(\omega/\alpha)^2 - k_z^2}$ with $\mathrm{Im}(k_\alpha) \le 0$ and $k_\beta = \sqrt{(\omega/\beta)^2 - k_z^2}$ with $\mathrm{Im}(k_\beta) \le 0$.

Note that when k_z equals zero, Eqs. (1) and (2) allow the calculation of the incident field provided by cylindrical linear loads (corresponding to the pure two-dimensional case).

When the system provided by the acoustic spaces inserted inside the elastic medium is exited by these loads, the resulting scattered field is obtained by using a Boundary Element model, previously developed by the authors [6]. The model used here makes use of Green functions for full fluid and elastic medium derived by Tadeu et al [5]. The final system of equations is manipulated so that the normal displacements and normal stresses are continuous, and null shear stresses are imposed along the boundary of the fluid-filled interfaces. This system of equations requires the evaluation of the following integrals along the discretized interfaces,

$$H_{ij}^{(s)kl} = \int_{C_l} H_{ij}^{(s)}(x_k, x_l, n_l)\, dC_l \;;\; i, j = 1, 2, 3 \quad (3)$$

$$H_{a_1}^{(a)kl} = \int_{C_l} H_{a_1}^{(a)}(x_k, x_l, n_l)\, dC_l$$

$$G_{ij}^{(s)kl} = \int_{C_l} G_{ij}^{(s)}(x_k, x_l)\, dC_l \;;\; i = 1, 2, 3;\; j = 1$$

$$G_{a_1}^{(a)kl} = \int_{C_l} G_{a_1}^{(a)}(x_k, x_l)\, dC_l, \quad (3)$$

in which $H_{ij}^{(s)}(x_k, x_l, n_l)$ and $G_{ij}^{(s)}(x_k, x_l)$ are the Green's tensor for traction and displacement components in the elastic medium, at point x_l in direction j caused by a point load acting at the source point x_k in direction i; $H_{a_1}^{(a)}(x_k, x_l, n_l)$ are the components of the Green's tensor for pressure in the fluid medium at point x_l, caused by a pressure load acting at the source point x_k; $G_{a_1}^{(a)}(x_k, x_l)$ are the components of the Green's tensor for displacement in the fluid medium, at point x_l in the normal direction, caused by a pressure load acting at the source point x_k; n_l is the unit outward normal for the l^{th} boundary segment C_l; the subscripts $i, j = 1, 2, 3$ denote the normal, tangential and z directions, respectively. Standard vector transformation operators are used to transform these equations from the x, y, z Cartesian coordinate system. The integrations needed for Equation (3) are carried out analytically for the loaded element [7, 8] and when the element to be integrated is not the loaded element, a Gaussian quadrature scheme is used.

3 Numerical simulations

3.1 Simulations description

The numerical simulations assume a geometry consisting of four acoustic quadrangular spaces divided by a wall with thickness h_p and a slab with thickness h_l. The elastic medium is made of ceramic material ($\alpha = 2182.2$ m/s; $\beta = 1336.3$ m/s; $\rho = 1400.0$ kg/m^3; $\eta = 1.5\times10^{-2}$). The properties of the acoustic medium correspond to air ($\rho_f = 1.22$ kg/m^3; $\alpha_f = 340.0$ m/s).

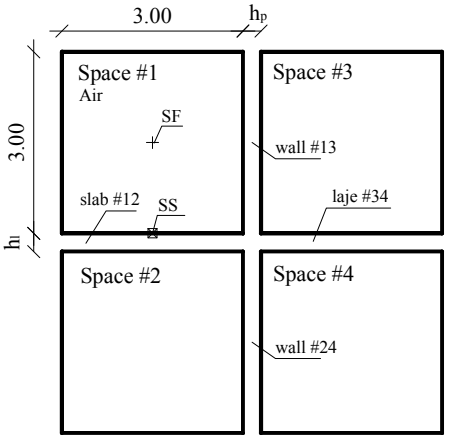

Fig.2 Geometry of the simulations.

With these simulations it is intended to investigate sound insulation due to flanking transmission. Therefore airborne sound insulation between space #1 and space #4, when a pressure source is placed in the acoustic space #1 (SF) was computed as well as impact sound pressure level registered in space #4 when a load acts in the slab # 12 along the vertical direction (SS).
Sound insulation results between contiguous space #1 and space #2 are also displayed to compare results.
The calculations were performed for a frequency range of [2.0;1410Hz] with a frequency step of 2.0 Hz. The pressure in the acoustic spaces was computed for a grid of receivers equally spaced of 0.25 m. Three lines of receivers equally spaced of 0.25 m were placed in the walls and slabs in order to calculate the vibration level of the separation elements.
The interfaces of the acoustic spaces are modeled with a number of boundary elements that increases with the excitation frequency of the harmonic source. The ratio between the wavelength of the incident waves and the length of the boundary elements is kept to a minimum of 7. Given the small distance between the two faces of the separating wall, the length of boundary elements modeling the wall is at least 4 times less than its thickness.

3.2 Airborne sound insulation

Fig. 3 displays the airborne sound insulation response obtained by computing the difference between the average sound pressure level in the emitting space (space #1) and in receiving space #2 (identified in the plot as R_{12}) when the partitions assume thicknesses of $h_p = h_l = 0.20$ m. This figure also shows the average sound insulation between space #1 and space #4 identified in the plot as R_{14}.

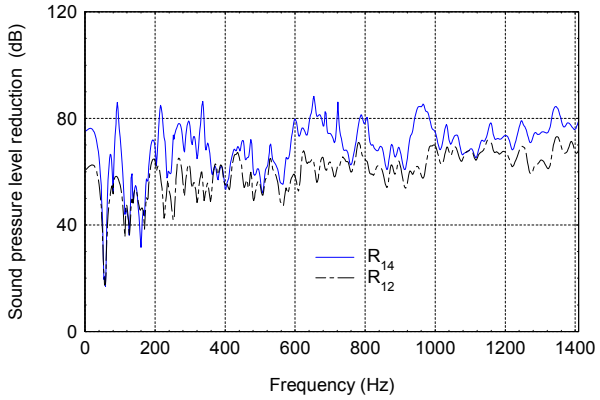

Fig.3 Airborne sound insulation response provided by the BEM model when $h_p = h_l = 0.20$ m.

From the analysis of the curves one observes that the sound pressure reduction between spaces #1 and #4, R_{14}, is higher than R_{12}, except for certain frequencies located below 150 Hz. At these frequencies (i.e. low frequencies) both curves approach as a result of the stationary field that is generated in the acoustic spaces and also due to the vibration modes of the structure.
Note that the sound pressure level that is generated in space #2 is due to the radiation of slab #12 (direct transmission) and from the radiation of the wall #24 (flanking transmission). On the other hand, the sound pressure level that reaches the receiving space #4, is due to the vibration of the wall #24 and slab #34 (flanking transmission). The cross junction that connects the walls and the slabs allows a reduction in the energy that is transmitted to these elements. As a result the sound pressure level reduction, R_{14}, is higher than R_{12}. Notice that the surrounding medium is infinite, therefore one assumes that the energy that is transmitted to the spaces using this path is neglected.

In order to better illustrate the acoustic behavior of the partitions, Fig. 4 displays the average vibration level of the wall and slab that radiate energy to space #2 (see Fig. 4a) and space #4 (see Fig. 4b).
The curves of Fig. 4 draw peaks at frequencies related to the acoustic and structural modes. Besides, from the analysis of Fig. 4a one concludes that the vibration level amplitudes regarding slab #12, are higher than that verified for wall #24, evidencing that the transmission to space #2 occurs mainly due to the vibration of the slab #12. Note also that at the low frequencies (bellow 150 Hz), the vibration level at certain frequencies is similar.

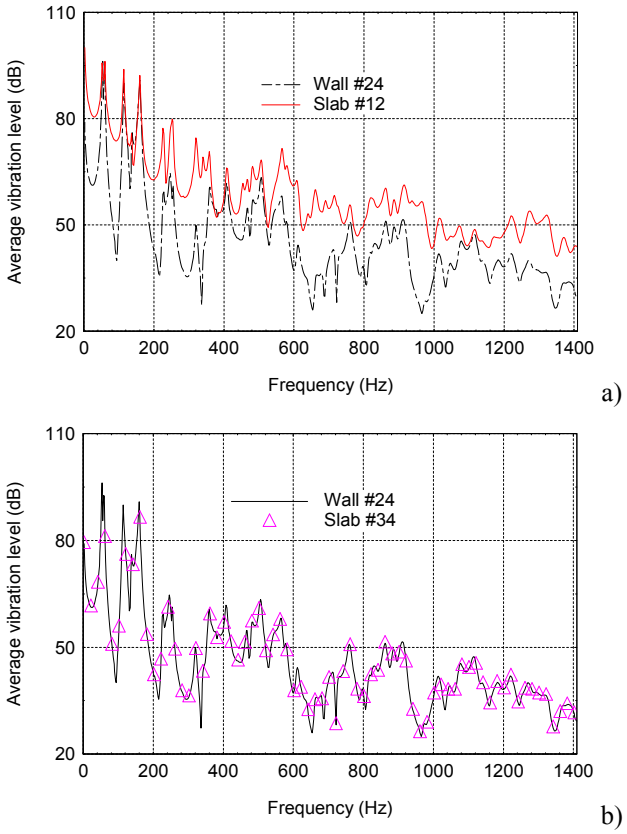

Fig.4 Average vibration level provided by the partitions with $h_p = h_l = 0.20$ m, that radiate energy to: a) space #2; b) space #4.

From the analysis of Fig. 4b it is seen that the vibration level regarding the wall #24 and the slab # 34 are similar and the corresponding amplitudes are lower than that computed for slab #12. As a result the sound pressure level recorded in space #4 is lower than that recorded in space #2.

3.3 Impact sound pressure level

Fig. 5 displays the impact sound pressure level recorded in space #2 and space #4 when a unit load acts at position

FS1. From the analysis of this figure we find that at certain frequencies located bellow 150 Hz, both levels are similar. However in the remaining frequency range the sound pressure level at space #2 is higher than that found in space #4.

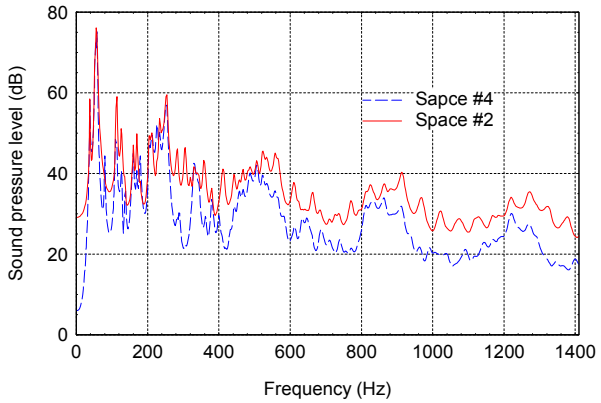

Fig.5 Impact sound pressure level response provided by the BEM model when $h_p = h_l = 0.20$ m .

Fig. 6 illustrates the average vibration level provided by the elements that radiate energy into space #2 (Fig. 6a) and space #4 (Fig. 6b).

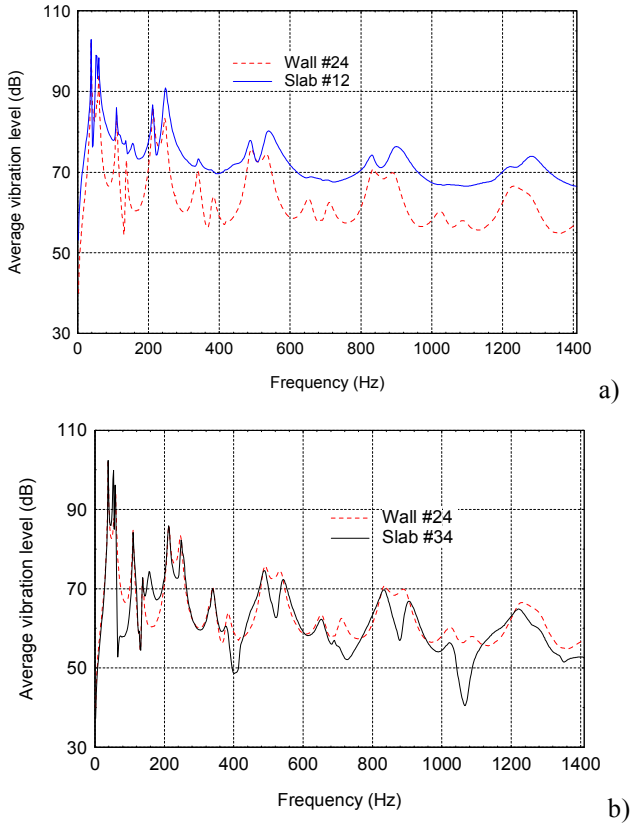

Fig.6 Average vibration level, provided by the partitions with $h_p = h_l = 0.20$ m , that radiate energy to: a) space #2; b) space #4.

From the analysis of the Fig. 6a one observes a set of peaks related with the vibration modes of the partitions. Besides, the vibration level provided by slab #12 evidences greater amplitudes than that obtained for wall #24, denoting that the main transmission path is given by the slab #12 (note that the impact is given in this slab). One can also observe that the peaks of the curve provided by slab #12 not always correspond to those regarding wall #24, evidencing a different vibration behavior between the wall and the slab. The curves plotted in Fig. 6b evidence that the amplitude of the vibration level provided by wall #24 and slab #34 approach and are smaller than that obtained for slab #12.

3.4 Influence of the stiffness of the structure

In this section the authors analyze the influence of the stiffness of the structure in the flanking transmission that reaches space #4, for varying thicknesses of the wall. Sound pressure level reduction results between space #1 and space #4 are plotted as well as the impact sound pressure level recorded in space #4. The analysis is performed using the results $h_l = h_p = 0.20$ m as a reference.

3.4.1 Airborne sound insulation

Fig. 7 displays sound pressure level reduction when the slab is $h_l = 0.20$ m thick and the thickness of the wall varies according to: $h_p = 0.20$ m , $h_p = 0.10$ m and $h_p = 0.30$ m .

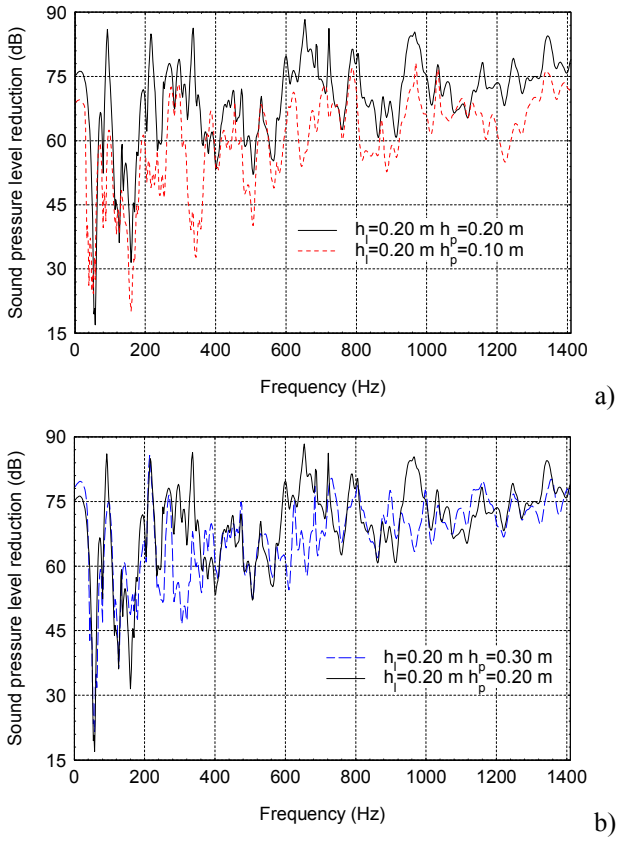

Fig.7 Sound pressure level reduction between space #1 and space #4 for: a) $h_p = h_l = 0.20$ m vs $h_p = 0.20$ m; $h_l = 0.10$ m ; b) $h_p = h_l = 0.20$ m vs $h_p = 0.20$ m; $h_l = 0.30$ m .

From the analysis of Fig. 7a we verify that when the thickness is $h_p = 0.10$ m , the sound pressure level reduction is lower in relation to the case where $h_p = 0.20$ m , for the majority of the frequencies. Both curves evidence the presence of dips in the frequencies related to the structural modes, however these dips are more pronounced when the thickness of the wall decreases. On

the other hand, when the thickness of the wall increases to $h_p = 0.30$ m (see Fig. 7b), the amplitudes of dips associated to the structural modes tend to decrease in relation to the case where $h_p = 0.20$ m. Besides in the higher frequencies, both curves tend to approach.
In order to make easier the comparison of the results the sound equivalent pressure level in spaces #1 and #4 for the different thicknesses was calculated for a frequency range between 89 Hz and 1410 Hz. The corresponding difference between the equivalent levels obtained in spaces #1 and #4 was computed subsequently. The results obtained were: $Dif = 31.4$ dB for $h_l = 0.20$ m, $h_p = 0.10$ m; $Dif = 42.1$ dB for $h_l = h_p = 0.20$ m and for $Dif = 51.1$ dB for $h_l = 0.20$ m, $h_p = 0.30$ m. From the analysis of these results we conclude that these difference increases has the thickness of the element increases.

3.4.2 Impact sound pressure level

Fig. 8 depicts the impact sound pressure level recorded in space #4 when the slab is $h_l = 0.20$ m thick and the thickness of the wall varies according to: $h_p = 0.10$ m, $h_p = 0.20$ m and $h_p = 0.30$ m. When the thickness of the wall decreases from $h_p = 0.20$ m to $h_p = 0.10$ m, the sound pressure level increase. On the other hand, when the thickness increases $h_p = 0.30$ m, the sound pressure level tends to decrease.

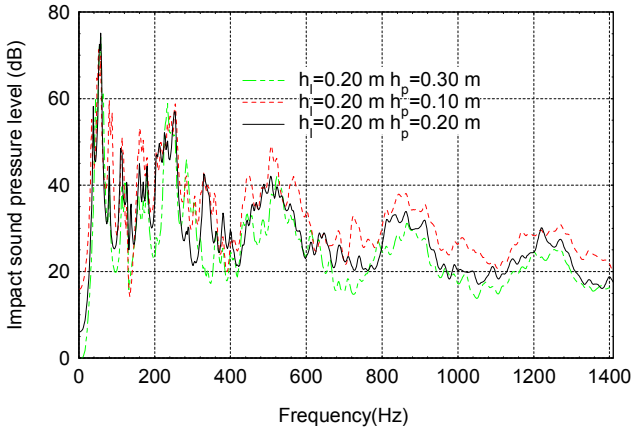

Fig.8 Impact sound pressure level in space #4.

The equivalent sound pressure level computed in space #4 is: $L_{eq}^{Fy} = 69.4$ dB for $h_l = 0.20$ m, $h_p = 0.10$ m; $L_{eq}^{Fy} = 66.5$ dB for $h_p = h_l = 0.20$ m; $L_{eq}^{Fy} = 66.7$ dB for $h_l = 0.20$ m, $h_p = 0.30$ m. These results do not vary significantly when compared with the airborne source results.

5 Conclusion

In this work a Boundary Element model was applied to assess sound insulation between non-adjacent rooms provided by single partitions. The analysis was performed in the low and medium frequency range.
When the load acts in the acoustic medium, the sound pressure level reduction between non-adjacent rooms is higher than that obtained for adjacent rooms, provided that the separating elements resemble. Moreover the transmission given by the wall and slab with the same thickness is alike. In the lower frequencies similar sound level reduction amplitudes were obtained due to the influence of the vibration modes of the rooms and of the structure. When the thickness of the wall decreased the sound level reduction between non-contiguous rooms decreased. On the other hand, when the thickness of the wall increased the sound pressure level reduction did not change significantly in relation to the situation when both partitions present the same thickness. These features denote that the sound insulation is influenced by the element with lower stiffness.
When the load acts in the elastic medium, the sound pressure level between non-contiguous rooms was found to be lower than that obtained for contiguous rooms, except at the low frequencies (bellow 150 Hz) where at certain frequencies both curves showed similar amplitudes.
When the thickness of the wall decreased the sound pressure level increased slightly. In fact when the thickness of the wall decreases the slab stiffness does not change significantly, therefore the corresponding curves only slightly shift upwards.

References

[1] E. Sewell, “Transmission of reverberant sound through a single leaf partition surrounded by an infinite rigid baffle”, *Journal of Sound and Vibration* 12, 21-32 (1970)

[2] B. Sharp, “Prediction methods for the sound transmission of building elements”, *Noise Control Engineering* 11, 53-63 (1978)

[3] L. Cremer, M. Heckl, E. Ungar, “Structure-Borne Sound”, Berlin, Springer-Verlag (1988).

[4] I. Vér “Impact noise isolation of composite floors”, *The Journal of the Acoustical Society of America* 50 (4), 1043-1050 (1970)

[5] A. Tadeu, E. Kausel,” Green’s functions for two-and-a half dimensional elastodynamic problems”, *Journal of Engineering Mechanics ASCE*, 126 (10), 1093-1097 (2000)

[6] A. Pereira, A. Tadeu, P. Santos, “Understanding the Effect of the Introduction of Structural Elements on 2D Structure - Borne Sound Propagation at Low Frequencies via BEM”, IAHS 31 International Association for Housing Science XXXI, CD ROM in \Housing Webpage\pdf\288.pdf, Montreal, Canadá, (2003)

[7] A. Tadeu, P. Santos, E. Kausel, “Closed-form integration of singular terms for constant, linear and quadratic boundary elements - Part I: SH Wave Propagation”, *Engineering Analysis with Boundary Elements*, 23 (8), 671-681 (1999)

[8] A. Tadeu, P. Santos, E. Kausel, “Closed-form integration of singular terms for constant, linear and quadratic boundary elements – Part II: SV-P Wave Propagation”, *Engineering Analysis with Boundary Elements*, 23 (9): 757-768 (1999)